Simulation of polyethylene oxide: Improved structure using better models for hydrogen and flexible walls

J. W. Halley, Yuhua Duan, and B. Nielsen
School of Physics and Astronomy, University of Minnesota, Minneapolis, Minnesota 55455

Paul C. Redfern and Larry A. Curtiss
Materials Science and Chemistry Divisions, Argonne National Laboratory, Argonne, Illinois 60439-4828

(Received 2 March 2001; accepted 31 May 2001)

We describe calculations of the structure of amorphous polyethylene oxide using a previously reported model, but with better treatment of hydrogen positions and in a code which allows relaxation of stresses in the polymerized sample by Rahman-Parrinello techniques. We also report the effects of two different intermolecular force field potentials and find that our earlier, empirical force field produces better agreement with experimental neutron scattering results than a force field derived from *ab initio* electronic structure calculations. © *2001 American Institute of Physics.*
[DOI: 10.1063/1.1386922]

I. INTRODUCTION

In a program to study the conductivity mechanisms of polymer electrolytes, we made a molecular dynamics study[1] of polyethylene oxide.[2] Though molecular dynamics studies have been done before,[3–6] our approach has some unique features. Here we report on an improved method for including hydrogen and/or deuterium in the model and show results using a modified form of the code which employs the Rahman-Parrinello methods to relax the stresses which are left after the computational polymerization which we use to make the amorphous model of the polymer. Both improvements have changed the structural predictions and we show that they now agree better with the neutron scattering experiments[7] than our previous calculations did. We compare the results with the neutron data previously reported in Ref. 7 where details of the experimental methods used can also be found. We chose to describe methyl and ethyl groups with the united atom model because including an explicit account of hydrogen motion in the molecular dynamics simulation would significantly increase the computational cost with little corresponding improvement in the accuracy of the structural or low frequency dynamical features which are of primary interest in our application. However, neutrons scatter strongly from hydrogen and deuterium, so the absence of hydrogen creates complications in the interpretation of neutron scattering experiments which are being carried out by our collaborators at Argonne National Laboratory.[7]

II. METHOD FOR INCLUDING HYDROGEN IN THE MODEL

To obtain an account of the effects of hydrogen or deuterium (which is substituted for hydrogen in the neutron scattering samples) we added hydrogen or deuterium to the model, not as a part of the full dynamical model, but only for the purposes of calculating the neutron scattering structure factors. (For simplicity we will refer to atom added as ''hydrogen'' in the rest of the formal account of the method. Within our approach, the only difference between hydrogen and deuterium is the mass. We present results in the last section using the deuterium mass, to account for the fact that the experimental data with which we compare is taken with a deuterated sample.) Because the CH distances are short and the CH stretch constant is large, the average positions of the hydrogen can be quite confidently predicted from the positions of surrounding carbon and oxygen centers. However, the rapid displacements of the hydrogen from their average positions due to quantum zero point motion are significant and must be included in some way in order to get a reasonable representation of the neutron scattering results. In previous papers[7,8] we reported results of a method in which we took approximate account of the zero point motion by displacing the hydrogen or deuterium centers from their average classical positions with random displacements obeying a spherically symmetric Gaussian distribution of about the right average displacement (roughly a tenth of an Angstrom).

On the other hand, it is not very difficult to make a better representation of these quantum displacements by taking account of the known nature of the force constants associated with the motions of CH_2 groups in a harmonic approximation.

A. Classical hydrogen positions

For each configuration in the classical molecular dynamics model described in Ref. 7 we determine average classical positions for hydrogen sites as illustrated in Fig. 1: At (united atom) carbon centers in the model which are not at the ends of polymer chains, first determine the O-C-C plane in which the carbon of interest is the one in the middle. Find the bisector of the (smallest) O-C-C angle in that plane and erect a plane, normal to the O-C-C plane and passing through that bisector. In this plane which is normal to the O-C-C plane, extend the aforesaid bisector to the side of the O-C-C complex containing the larger O-C-C angle in the O-C-C plane and place the two average hydrogen positions symmetrically about the bisector, so that the angular separation between the

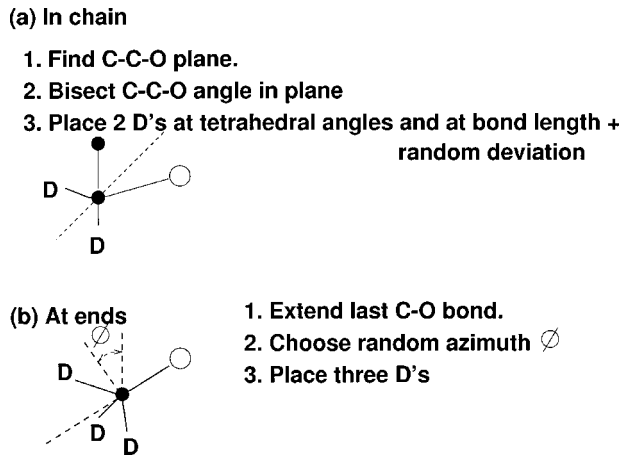

FIG. 1. Determination of H/D positions. Open circles: O; filled circles: CH_2 or CH_3.

two CH bonds is the tetrahedral angle and the CH distances are the standard value of 1.68 Å. In the case of (united atom) carbon atoms which are at the ends of chains, extend a line through the last O-C bond in the chain beyond the end of the chain. Determine an azimuthal angle by drawing a random number from a uniform distribution between 0 and 2π and add 3 hydrogen/deuterium atoms at the standard CH bond length in such a way that the angles between CH bonds are all the tetrahedral angle and such that the resulting HHHO tetrahedron is oriented azimuthally as illustrated in Fig. 1.

Previously,[7,8] we choose a position for each hydrogen which differed from the average value by selecting a random displacement with an isotropic Gaussian probability distribution of width 0.1 Å. A better method utilizes the approximately known harmonic force constants characterizing the motions of the CH groups.[9] These force constants vary from polymer to polymer and probably depend weakly on polymer configuration and on whether one is looking at the end of a chain or in the middle of a chain. Nevertheless, because the frequency of most of the CH modes is high relative to the frequencies of other vibrational and relaxational modes of the polymer, it is a reasonable approximation to ignore these variations for our purposes.

B. Model for quantum model of hydrogens

We describe the harmonic motions of a pair of hydrogen atoms as illustrated in Fig. 2 in terms of a coordinate system in which the x-axis is perpendicular to the OCC plane, the *z*-axis lies along the bisector of the two CH bonds for the average H positions and the *y*-axis is perpendicular to the *x* and *z* axes. The directions of the axes of this local coordinate system for each C center not at the end of a chain are determined from the coordinates of the centers in the program coordinate system as follows: Let $\vec{r}_{\mathrm{O,C}}$ and $\vec{r}_{\mathrm{C}',\mathrm{C}}$ be vectors from the C center of interest to the neighboring oxygen (O) and carbon centers (C′). Then the unit vectors $\hat{x},\hat{y},\hat{z}$ which form the axes of the local coordinate system in Fig. 2 are given by

$$\hat{x}=\frac{\vec{r}_{\mathrm{O,C}}\times\vec{r}_{\mathrm{C}',\mathrm{C}}}{|\vec{r}_{\mathrm{O,C}}\times\vec{r}_{\mathrm{C}',\mathrm{C}}|}, \tag{1}$$

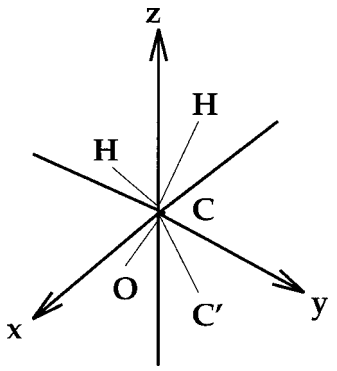

FIG. 2. Coordinate system as discussed in the text.

$$\hat{z}=-\frac{\vec{r}_{\mathrm{O,C}}+\vec{r}_{\mathrm{C}',\mathrm{C}}}{|\vec{r}_{\mathrm{O,C}}+\vec{r}_{\mathrm{C}',\mathrm{C}}|}, \tag{2}$$

$$\hat{y}=\hat{z}\times\hat{x}. \tag{3}$$

The harmonic motions can then be described as stretching (force constant K_s), scissors (force constant K_{sciss}) twisting (force constant K_ϕ), wagging (force constant K_ψ) and rocking (force constant K_α). The harmonic potential energy describing hydrogen motions is written:

$$\begin{aligned}V=&(K_s/2)[(\vec{r}_{\mathrm{H1}}-a)^2+(\vec{r}_{\mathrm{H2}}-a)^2]\\&+(K_{\mathrm{sciss}}/2)(\theta_{12}-\theta_0)^2+[K_\psi/2(\psi)^2]\\&+(K_\phi/2)(\phi^2)+(K_\alpha/2)\alpha^2,\end{aligned} \tag{4}$$

where a is the equilibrium C-H distance. Appropriate approximate values for the frequencies are taken from Ref. 9 and shown in Table I. The angles in (4) are easily related to coordinates defined in Fig. 2 as follows:

$$\psi=\arctan\left[\frac{(\vec{r}_{\mathrm{H1}}\times\vec{r}_{\mathrm{H2}})\cdot\hat{z}}{(\vec{r}_{\mathrm{H1}}\times\vec{r}_{\mathrm{H2}})\cdot\hat{y}}\right], \tag{5}$$

$$\phi=\arctan\left[\frac{(\vec{r}_{\mathrm{H1}}\times\vec{r}_{\mathrm{H2}})\cdot\hat{x}}{(\vec{r}_{\mathrm{H1}}\times\vec{r}_{\mathrm{H2}})\cdot\hat{y}}\right], \tag{6}$$

$$\theta=\arccos\left(\frac{\vec{r}_{\mathrm{H1}}\cdot\vec{r}_{\mathrm{H2}}}{r_{\mathrm{H1}}r_{\mathrm{H2}}}\right), \tag{7}$$

$$\alpha=\arccos(\hat{z}'\cdot\hat{z}). \tag{8}$$

Here $\vec{r}_{\mathrm{H1}}$ and $\vec{r}_{\mathrm{H2}}$ are vectors with the direction and length of the two CH bonds. A unit vector along the instantaneous bisector of these two unit vectors, $\hat{z}'$ is projected onto the zx plane. We obtain the potential energy of V of Eq. (4) in terms of the coordinate system defined in Fig. 2 by use

TABLE I. Values of frequencies and force constants used.

Mode	Frequency (f in cm^{-1})	Force Constant ($\omega=2\pi f\times c$)
Rocking	900	$K_\alpha=2\times m_{\mathrm{H,D}}\omega^2$
Scissors	1500	$K_{\mathrm{sciss}}=2\times m_{\mathrm{H,D}}\omega^2$
Wagging	1350	$K_\psi=2\times m_{\mathrm{H,D}}\omega^2$
Twist	1225	$K_\phi=2\times m_{\mathrm{H,D}}\omega^2$
Stretch	3000	$K_s=m_{\mathrm{H,D}}\omega^2$

of these relations by expanding Eqs. (5)–(8) for small displacements of the vectors $\vec{r}_{H1}$ and $\vec{r}_{H2}$ about the average positions of the H centers. Then one finds

$$V = K_s/2\left[\delta x_1^2 \sin^2\frac{\theta_0}{2} + \delta z_1^2 \cos^2\frac{\theta_0}{2} - 2\,\delta x_1 \delta z_1 \cos\frac{\theta_0}{2}\sin\frac{\theta_0}{2}\right]$$
$$+ K_s/2\left[\delta x_2^2 \sin^2\frac{\theta_0}{2} + \delta z_2^2 \cos^2\frac{\theta_0}{2}\right.$$
$$\left. - 2\,\delta x_2 \delta z_2 \cos\frac{\theta_0}{2}\sin\frac{\theta_0}{2}\right]$$
$$+ K_{\text{sciss}}/2\left[\left(\frac{\delta x_1 - \delta x_2}{a}\right)\cos\frac{\theta_0}{2} + \left(\frac{\delta_{z1} + \delta_{z2}}{a}\right)\sin\frac{\theta_0}{2}\right]^2$$
$$+ \frac{K_\phi}{8}\left[\left(\frac{\delta_{y1} - \delta_{y2}}{a}\right)^2 \frac{1}{\sin^2\frac{\theta_0}{2}}\right]$$
$$+ \frac{K_\psi}{8}\left[\left(\frac{\delta_{y1} + \delta_{y2}}{a}\right)^2 \frac{1}{\cos^2\frac{\theta_0}{2}}\right]$$
$$+ \frac{K_\alpha}{8a^2\cos^2\frac{\theta_0}{2}}[(\delta x_1 + \delta x_2)^2 + \tfrac{3}{4}(\delta z_1 + \delta z_2)^2]. \tag{9}$$

Here $\delta x_{1,2}, \delta y_{1,2}, \delta z_{1,2}$ are the displacements of the two vectors describing the positions of the two H centers in question (measured from the common C center) relative to the average positions and expressed in the coordinate system of Fig. 2. Specifically, the relation is

$$\vec{r}_{H1} = \left(-a\sin\frac{\theta_0}{2} + \delta x_1, \delta y_1, a\cos\frac{\theta_0}{2} + \delta z_1\right), \tag{10}$$

$$\vec{r}_{H2} = \left(a\sin\frac{\theta_0}{2} + \delta x_2, \delta y_2, a\cos\frac{\theta_0}{2} + \delta z_2\right), \tag{11}$$

the potential energy in the general form

$$V = \left(\frac{1}{2}\right)\sum_{i,\nu;j,\mu} K_{i,\nu;j,\mu}\delta x_{i,\nu}\delta x_{j,\mu}, \tag{12}$$

where i refers to atomic sites and ν, μ refer to Cartesian directions x,y,z. The equation of motion within the harmonic approximation used for the H center motion is then classically

$$M_H\frac{d^2\delta x_{i,\nu}}{dt^2} = \sum_{j,\mu} K_{i,\nu;j,\mu}\delta x_{j,\mu}, \tag{13}$$

with harmonic angular eigenfrequencies ω_λ given by solutions of the eigenvalue equation

$$|M_H\omega_\lambda^2\delta_{i,\nu,j,\mu} - K_{i,\nu;j,\mu}| = 0. \tag{14}$$

Eigenvectors $u_\lambda = \Sigma_{i,\nu} A_{i,\nu}^\lambda \delta x_{i,\nu}$ oscillate independently with frequencies ω_λ in the classical case if the coefficients $A_{i,\nu}^\lambda$ satisfy

$$\sum_{j,\mu}(M_H\omega_\mu^2\delta_{i,\nu;j,\mu} - K_{i,\nu;j,\mu})A_{j,\mu} = 0. \tag{15}$$

Quantizing these harmonic oscillator modes in the well known way,[10] one obtains the quantum Hamiltonian

$$H_Q = \sum_\lambda \hbar\omega_\lambda a_\lambda^\dagger a_\lambda, \tag{16}$$

in which the creation and annihilation operators $a_\lambda^\dagger$ and a_λ are related to the displacements u_λ through the relation

$$u_\lambda = \sqrt{\frac{\hbar}{2M_{H,D},\omega_\lambda}}(a_\lambda^\dagger + a_\lambda), \tag{17}$$

at zero temperature it follows that the expectation value $\langle u_\lambda^2\rangle$ is

$$\langle u_\lambda^2\rangle = \frac{\hbar}{2M_{H,D}\omega_\lambda}, \tag{18}$$

whereas at finite temperatures

$$\langle u_\lambda^2\rangle = \frac{\hbar}{2M_{H,D}\omega_\lambda}\coth(\hbar\omega_\lambda/2k_BT). \tag{19}$$

The relation of u_λ to displacements defined in the coordinate system defined in Fig. 2 is

$$u_\lambda = \sum_{i,\mu} A_{i,\mu}^\lambda \delta x_{i,\mu}. \tag{20}$$

Inverting this relation:

$$\delta x_{i,\mu} = \sum_\lambda (A^{-1})_{i,\mu}^\lambda u_\lambda, \tag{21}$$

from which one obtains the matrix describing the fluctuations of the hydrogen/deuterium positions in the coordinate system of Fig. 2:

$$\langle \delta x_{i,\mu}\delta x_{j,\nu}\rangle = \sum_\lambda (A^{-1})_{i,\mu}^\lambda (A^{-1})_{j,\nu}^\lambda \langle u_\lambda^2\rangle, \tag{22}$$

inverting this matrix we obtain the probability distribution from which deviations of the hydrogen/deuterium positions from the average positions in the coordinate system of Fig. 2:

$$P(\{\delta x_{k,\gamma}\}) \propto \exp\left(-\sum_{i,\mu;j,\nu}\delta x_{i,\mu}\delta x_{j,\nu}(\langle\delta x\,\delta x\rangle^{-1})_{i,\mu;j,\nu}\right). \tag{23}$$

The algorithm for selecting deviations from average positions is then as follows:

1. Diagonalize the matrix (14) and compute the eigenvectors (this need only be done once) giving the ω_λ, $A_{i,\nu}^\lambda$ and the matrix $(\langle\delta x\,\delta x\rangle^{-1})_{i,\mu;j,\nu}$ (by inversion of the sum in equation).
2. During the molecular dynamics run, at each time when data are collected for computation of radial distribution functions (typically not every time step) determine average positions for H centers as in Sec. II above.
3. For each pair of H centers select 6 random numbers between zero and 1, denoted $r_{1,x},\ldots,r_{2,z}$. From these compute candidate displacements $\delta x_{i,\mu} = \delta a \times (r_{i,\mu} - 0.5)$

TABLE II. Values of the Intermolecular Force Field Parameters: The force field potential has the Lennard-Jones form $A/r^{12}-B/r^6$. Only constants for like centers are shown. For unlike centers we used the geometric averages as explained in Ref. 1. For example $A_{\text{O-CH}_2}=\sqrt{A_{\text{O-O}}A_{\text{CH}_2\text{-CH}_2}}$ Units are A (kcal Å^{12}), B (kcal Å^6). The effective charges for the Coulomb interaction were O(-0.326|e|), C(0.163|e|) for both models.

	A_{OO}	$A_{\text{CH}_2\text{-CH}_2}$	$A_{\text{CH}_3\text{-CH}_3}$	B_{OO}	$B_{\text{CH}_2\text{-CH}_2}$	$B_{\text{CH}_3\text{-CH}_3}$
Empirical	109,590	1,272,800	2,516,600	204.06	781.64	1 228.8
Ab initio	476 616.9	5,934,641	8,171,486	569.297	1673.7	2 286.865

where δa is an amplitude chosen to make the probability of acceptance at the next step reasonably high. (Characteristically we used values of δa of the order of 0.1 Å.) Evaluate the (unnormalized) probability $p=\exp[-\Sigma_{i,\mu;j,\nu}\delta x_{i,\mu}\delta x_{j,\nu}(\langle\delta x\delta x\rangle^{-1})_{i,\mu;j,\nu}]$ [see Eq. (23)]. Select another random number r evenly distributed between 0 and 1. If $r<p$, accept the trial displacements for this pair.[11] Otherwise repeat step 3.

4. Repeat 1 through 3 for all C centers.

III. SIMULATION AT CONSTANT PRESSURE

We have also improved the code describing amorphous polyethylene oxide by implementing a simulation of it at constant pressure, using the method due to Rahman and Parrinello.[12] Because their formulation was for systems containing only two body forces, it was necessary to extend the Rahman-Parrinello algorithms for use with the three body torsion forces present in our polyethylene oxide model. (The treatment of long range Coulomb interactions via Ewald simulations also requires some care when it is implemented in the Rahman-Parrinello scheme but this has been discussed elsewhere).[13] Though this implementation has been done before,[13] we briefly reiterate our approach. In the language of Ref. 2, we define the matrix $\mathbf{h}$ from 3 vectors $\vec{a},\vec{b},\vec{c}$ which define the periodically continued simulation celli. The columns of $\mathbf{h}$ are the components of $\vec{a},\vec{b},\vec{c}$ as in Ref. 12. We permit these to move dynamically at fixed pressure. The dynamical variables are the elements of $\mathbf{h}$ and $\vec{s}_i$ for particles $i=1, N$ and where $\vec{s}_i=\xi_i,\eta_i,\zeta_i$ define the particle positions $\vec{r}_i$ through the relation $\vec{r}_i=\xi_i\vec{a}+\eta_i\vec{b}+\zeta_i\vec{c}=\mathbf{h}\vec{s}_i$. The Lagrangian from which the equations of motion are derived is

$$L=\left(\frac{1}{2}\right)\sum_{i=1}^{N} m_i\dot{\vec{s}}_i^T\mathbf{G}\dot{\vec{s}}-V(\vec{r}_1,\ldots,\vec{r}_N)+\left(\frac{1}{2}\right)Tr\dot{\mathbf{h}}^T\dot{\mathbf{h}}-p\Omega, \tag{24}$$

in which $\Omega=\vec{a}\cdot(\vec{b}\times\vec{c})$ is the (time varying) cell volume. This is the same Lagrangian as that defined in Ref. 12 except that the potential V is permitted to be an arbitrary function of the particle positions, instead of being a sum of pair potentials. As in Ref. 12, $\mathbf{G}=\mathbf{h}^T\mathbf{h}$. We denote the Euclidean components of the force on the particle i by $F_{\lambda,i}=-\partial V/\partial r_{\lambda,i}$. Then the equations of motion for the variables $\vec{s}_i$ and $\mathbf{h}$ take the form

$$\ddot{s}_{\lambda,i}=-G^{-1}_{\lambda\mu}\dot{G}_{\mu\nu}\dot{s}_{\nu i}+G^{-1}_{\lambda\mu}h^T_{\mu\nu}F_{\nu i}, \tag{25}$$

$$W\ddot{\mathbf{h}}_{\lambda\mu}=\sum_i m_i v_{i\lambda}\dot{s}_{\mu i}-p\Omega h^{T^{-1}}_{\lambda\mu}-\sum_i F_{\lambda,i}s_{\mu i}. \tag{26}$$

Here we have used the summation convention for repeated greek indices. In these equations, $\vec{v}_i=\mathbf{h}\dot{\vec{s}}_i$ as in Ref. 12. The equations can be shown to be identical to those of Ref. 12 except for the last term in each, which has been expressed in a more general form, appropriate for calculation with forces of any type which can be derived from a potential which is a function only of the particle coordinates. If we specialize to forces derived from pair potentials, we again recover the equations of Ref. 12 exactly.

IV. *AB INITIO* FORCE FIELDS

In Ref. 1 we used force fields estimated from the literature to describe the nonbonding forces between the monomers of the polymer. Recently, we have fitted first principles *ab initio* results for the interaction of two diglyme units of PEO to Lennard-Jones potential of the form we are using in these simulations and have obtained a different parametrization, as summarized in Table II. We will report results for both parametrizations in the following. For both the *ab initio* and the empirical force fields, we use different interactions for the methyl carbons at the ends of chains and for the ethyl carbons along the chains. [In comparisons with experiment, this is somewhat unrealistic because our computational samples contain many more end groups than the real polymer. However, we have found that the calculated $g(r)$ described below is essentially unchanged if we use the ethylene force field parameters for all the monomers in our computational sample so this error has no effects at least for $g(r)$.]

The Lennard-Jones (LJ) potential parameters were obtained from fitting of a potential energy curve for the interaction of two diglyme molecules generated from the *ab initio* molecular orbital calculations. The points on the surface were obtained from second-order perturbation theory using the 6-311G** basis set (MP2/6-311G**).[14] The *ab initio* potentials are very similar to ones derived from LJ potentials reported by Jorgenson and Tirado-Rives[15] from fitting to organic liquid data. Since the latter potentials are essentially the same as the *ab initio* one, they would likely give similar results for the radial distribution functions as the *ab initio* potential if MD simulations were carried out with them.

V. RESULTS

The general approach in this project is to polymerize the model computationally, starting with the monomeric fluid, and to use the rate at which the polymerization is done as a control parameter in order to match the (nonequilibrium) structure found in experiment. In the results reported here, all the samples were simulated for about 2 ps after polymeriza-

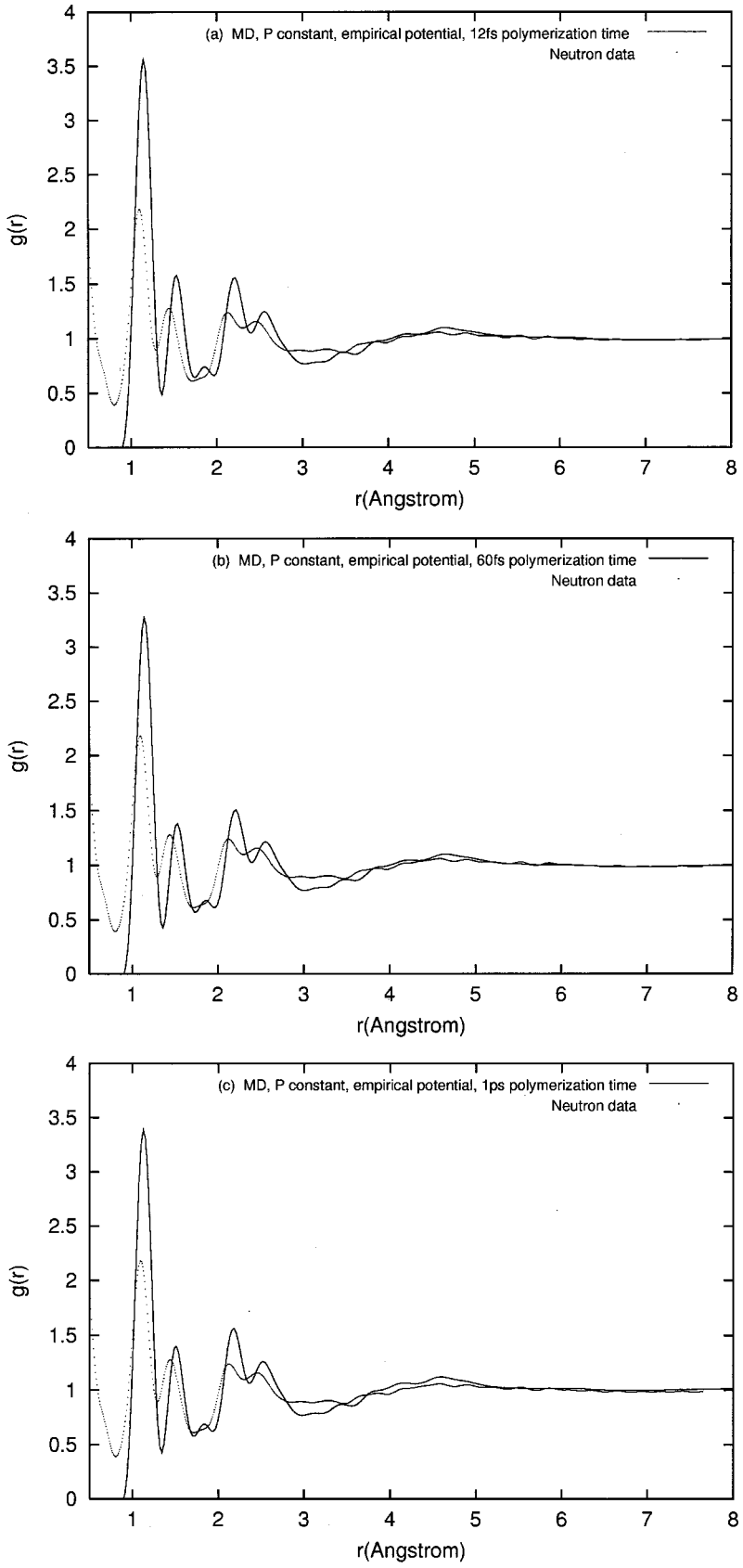

FIG. 3. Comparison of radial distribution function from model described here for various polymerization rates with the neutron scattering results. Times between computation ''polymerization'' events are: (a) 12 fs, (b) 60 fs, and (c) 1 ps.

tion and then for at least 20 ps to collect data. We ran some simulations for 80 ps and did not observe significant differences in the calculated structure $g(r)$. Sample sizes were the same as in Refs. 1 and 7. Constant volume calculations were carried out at a volume of $(24.206)^3$ Å^3 corresponding to a density of 1.165 gm/cm^3, quite close to the experimental density of 1.158 gm/cm^3 and giving a computed pressure of ≈ -4 atm. Constant pressure runs were carried out at a pres-

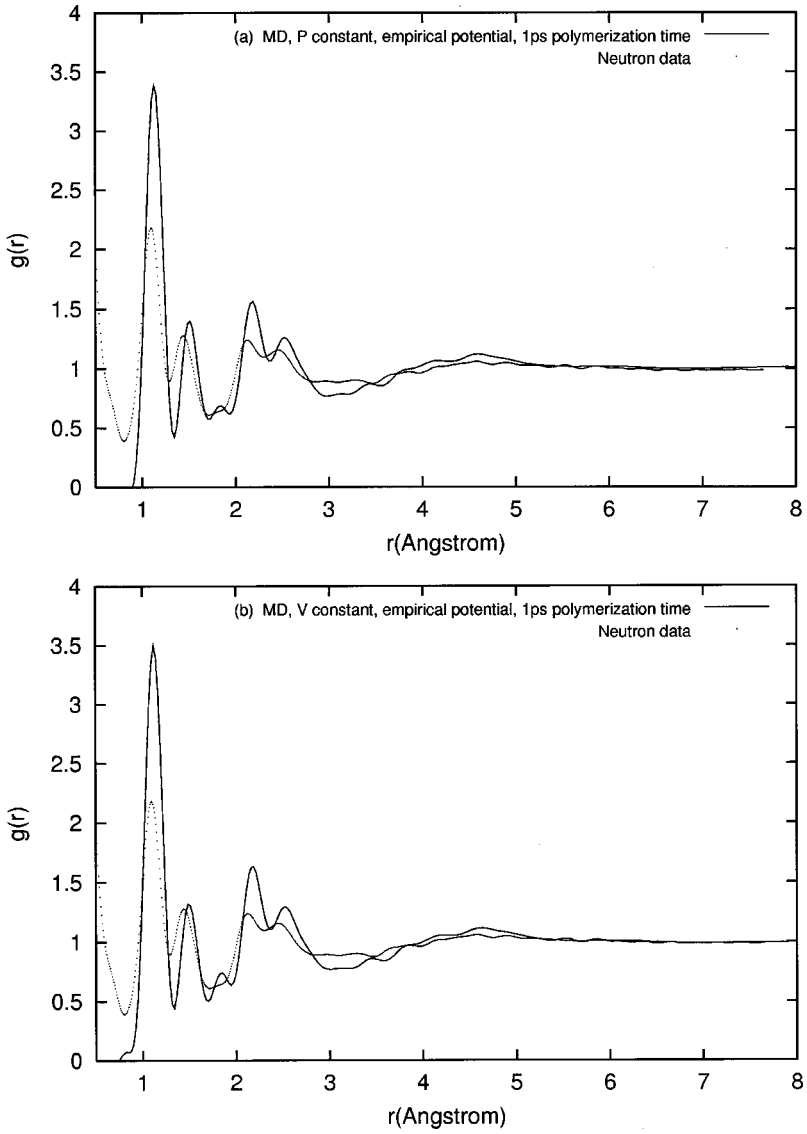

FIG. 4. Effect of constant pressure vs constant volume on the radial distribution function results: (a) constant pressure, and (b) constant volume.

sure of 1 atm, giving a computed volume of $(24.152)^3$ Å^3 and nearly the same density. A simple thermostat held the average kinetic energy at a value corresponding to 400 K. We present results for several computational polymerization rates as summarized in Fig. 3 using the empirical force fields, the new method for treating hydrogen and the simulation at constant pressure. The differences between the results for the three different polymerization rates are small but the results for a time between polymerization events of 1 ps are in slightly better agreement with the experimental results. In computational samples polymerized at this rate, there were characteristically around 15 chains with lengths in the range 6 to 32 monomers. In the next three Figs. 4–6, we show the effects of the three new features introduced in the computations carried out here. Figure 4 compares the result at constant pressure and at constant volume, both with the empirical force fields, a 1 ps polymerization time and the full assymmetric distribution for the deuterium positions.

The constant pressure results are in significantly better agreement with the experiments than the constant volume ones. Figure 5 shows the effect of nonspherical distribution of hydrogen around the classical positions. Here we compare results with constant pressure, a 1 ps polymerization time and the empirical force fields with the full asymmetric and the spherical Gaussian distributions of deuterium positions. The differences are not significant. Finally, in Fig. 6 we show the effect of using the *ab initio* force fields by comparing the results at constant pressure, 1 ps polymerization time and assymetric distributions of deuterium for the empirical and *ab initio* force fields. It is clear that the *ab initio* force fields do not give results which agree as well with the experiments as the empirical force fields do.

To obtain these results, we have calculated the experimentally observed[7] linear combination of partial radial distribution functions,

$$g_{md}(r)=\sum_{\alpha,\beta} c_\alpha c_\beta g_{\alpha\beta}(r), \tag{27}$$

from the MD code and the two algorithms for adding hydrogen as described above and have then convoluted the result with the appropriate Fourier transform of the Lorch window function used in the analysis of the experiments. Details of the convolution procedure appear in the Appendix.

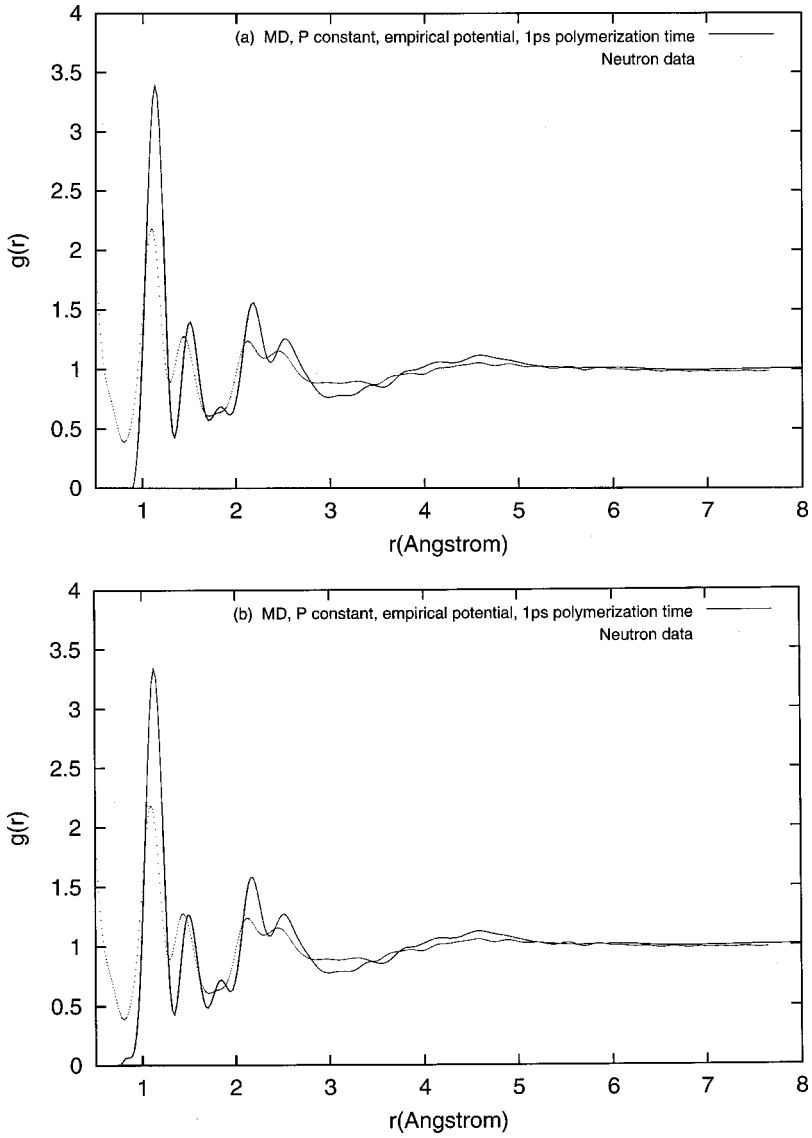

FIG. 5. Effect of improved description of hydrogen motion on the radial distribution function results: (a) results with aspherical distribution as described here. (b) Results with previous spherical Gaussian distribution.

VI. CONCLUSIONS

We have introduced a new procedure for taking account of the presence of hydrogen in molecular dynamics simulations of hydrocarbons, without sacrificing the advantages of the united atom model for methyl groups in speeding up the trajectory calculations. The method takes account of important zero point effects in the motion of the hydrogen atoms, without involving the significantly increased computational cost of including them by path integral or related methods. Like some of those methods, this approach is only useful for calculating structural features of the simulated system. Some authors have reported artificially weakening the C–H bond strengths in a classical simulation model which explicitly includes hydrogen motion, in order to produce hydrogen motion approximately like the quantum zero point motion. This is much less realistic than the present method and is, computationally, significantly more expensive. We have also improved the model by simulating at constant pressure and have explored the effects of using force fields derived from first principles electronic structure calculations.

We applied our method to a previously reported model for amorphous polyethylene and compared the results with neutron scattering results on that system. The biggest change in the simulation results (and which significantly improved the model as a representation of the neutron data) arose from the introduction of the constant pressure algorithm (Fig. 4). By contrast, improved treatment of hydrogen (Fig. 5) and varying the polymerization rate (Fig. 3) had small effects on the structure. A somewhat surprising aspect of the results is that the empirical force fields used to describe interchain interactions in our earlier work seem to describe the experimental neutron data better than the presumably better force fields derived from first principles electronic structure (Fig. 6). The reasons for this are not entirely clear particularly because the first principles force fields agree with empirical results of Jorgenson,[15] which were derived by fitting molecular dynamics data on monomeric liquids. We compare the force field potentials in Fig. 7. Our empirical force field potentials which were taken from an earlier empirical model[16] are ''softer.'' That is, the sharp rise to positive potentials at short distances occurs at smaller separations and is less steep than in the potentials derived from first principles calcula-

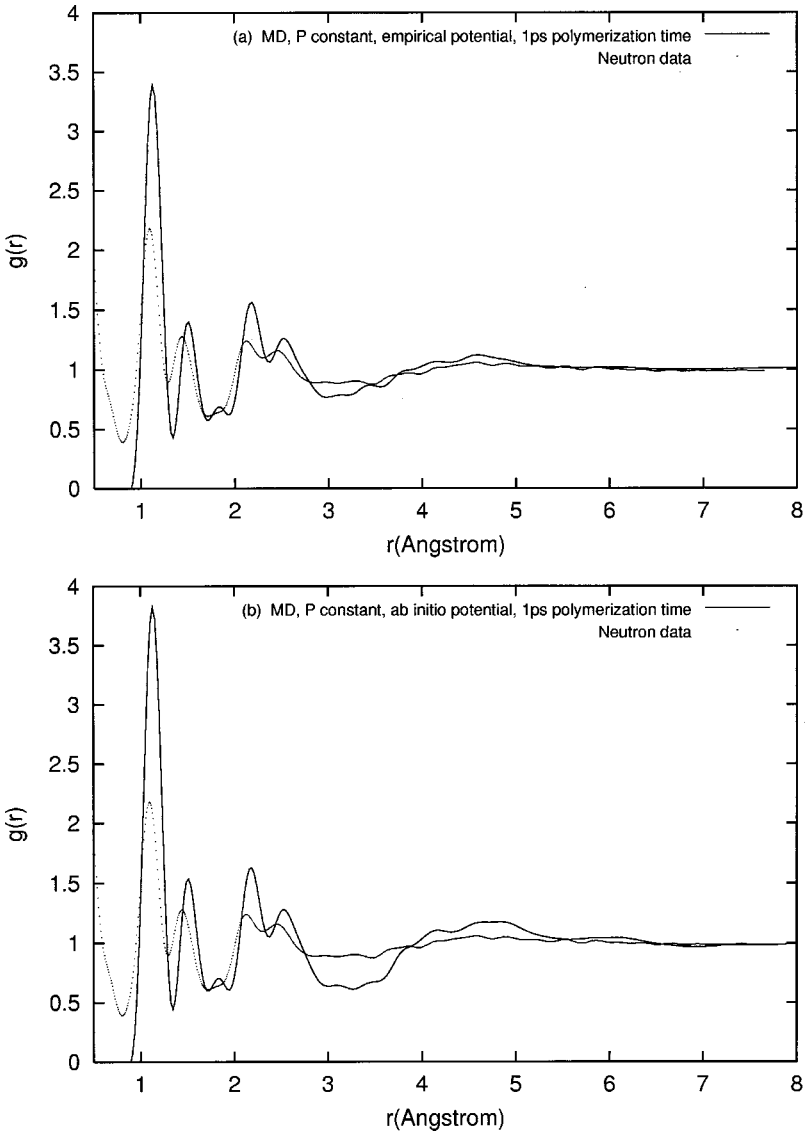

FIG. 6. Effect of new force field potentials: (a) $g(r)$ calculated with empirical potentials, and (b) with *ab initio* force field potentials.

tions. Possibly the force fields which were derived from interactions between short, diglyme molecules are not representative of forces between longer chains. (We have made some preliminary *ab initio* calculations with different configurations and larger molecules which suggest that the forces may indeed be less repulsive on average than those given by the fit to *ab initio* data used here.) Finally, there are discrepancies between the data and the calculations at the shortest distances in all the radial distribution functions. In particular, the weight under the C-D peak at around 1 Å is smaller in the calculations than in the experimental data. Because we have carefully checked that the weight under the C-D peak is consistent with the number of deuterium in the simulation, it seems likely that this discrepancy is due to some kind of experimental artifact in the data at short distances.

ACKNOWLEDGMENTS

This work is supported in part by the Division of Chemical Sciences, Office of Basic Energy Sciences, of the Department of Energy through Grant No. DE-FG02-93ER14376, by the Division of Chemical Sciences, Office of Basic Energy Sciences, U.S. Department of Energy, under Contract No. W-31-109-ENG-38 and by the University of Minnesota Supercomputing Institute.

APPENDIX: CONVOLUTION OF MD DATA FOR COMPARISON WITH EXPERIMENT

The neutron scattering structure factor $S(Q)$ is used to obtain a radial distribution function $g(r)$ by use of the expression

$$g(r)=1.0+1/\rho\int[S(Q)-1]W(Q)e^{i\vec{Q}\cdot\vec{r}}\frac{d\vec{Q}}{(2\pi)^3},$$

which is the standard expression except for a window function $W(Q)$ which was taken to have the Lorch form

$$W(Q)=\frac{\sin(Q\pi/Q_{\max})}{Q\pi/Q_{\max}},$$

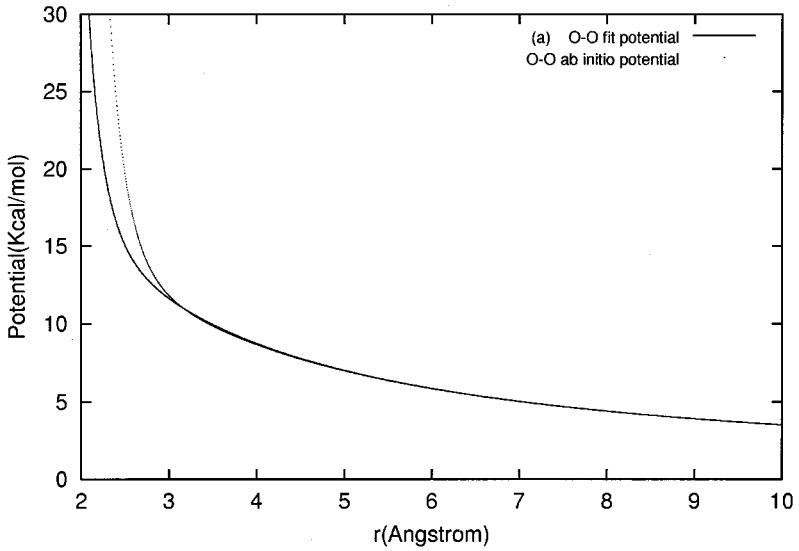

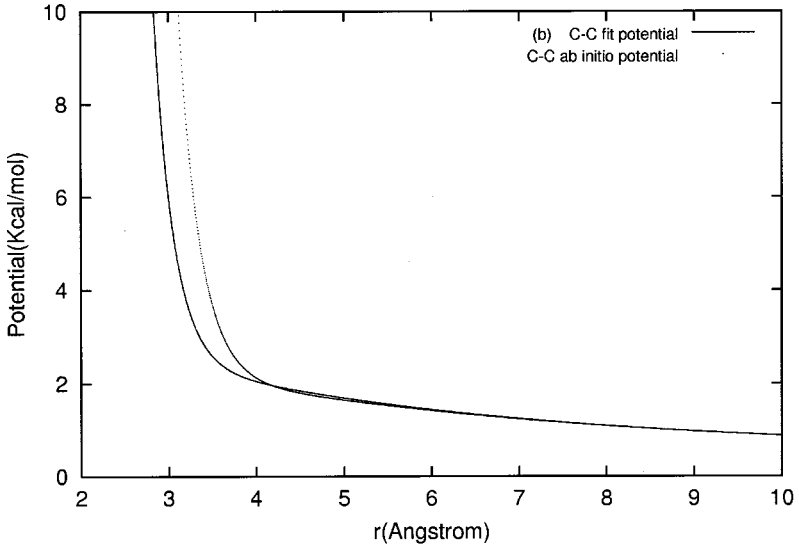

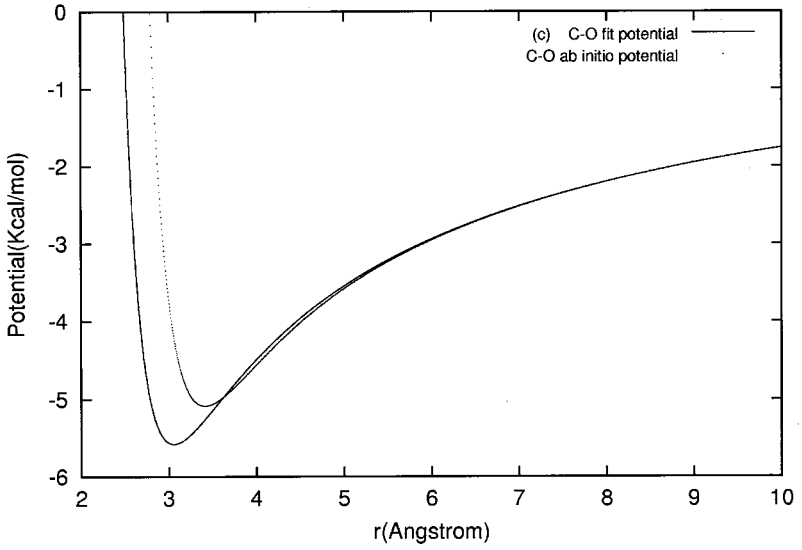

FIG. 7. Comparison of empirical and first principles interchain force field potentials: (a) O–O potential, (b) C–C potentials, and (c) C–O potentials.

for $Q<Q_{\max}$ and zero otherwise. The formal relation between the calculated radial distribution function $g_{md}(r)$ and the structure factor $S_{md}(Q)$ is given by the same relation without the window function

$$g_{md}(r)=1.0+1/\rho\int[S_{md}(Q)-1]e^{i\vec{Q}\cdot\vec{r}}\frac{d\vec{Q}}{(2\pi)^3}.$$

To obtain a calculated quantity $\tilde{g}_{md}(r)$ for comparison with

the experimental $g(r)$, we formally invert the last equation:

$$[S_{md}(Q)-1]/\rho=\int e^{i\vec{Q}\cdot\vec{r}}[g_{md}(r)-1]d\vec{r}.$$

Then multiplying this result by $W(Q)\rho$ and Fourier transforming back as in the experimental relation, we obtain

$$\tilde{g}_{md}(r)=1.0+1/\rho\int [S_{md}(Q)-1]W(Q)e^{i\vec{Q}\cdot\vec{r}}\frac{d\vec{Q}}{(2\pi)^3}.$$

Then by use of the last two equations, rearranging and carrying out the integrals on wave vector explicitly, one has

$$\vec{g}_{md}(r)=1.0+\int dr'F(r')\times\int_{-1}^{+1}(g_{md}(\sqrt{r''^2+r^2-2r''r\mu})-1)d\mu,$$

in which

$$F'(r')=\frac{Q_{\max}^2 r'}{2\pi^2}\left[\frac{\sin(Q_{\max}r'-\pi)}{Q_{\max}r'-\pi}-\frac{\sin(Q_{\max}r'+\pi)}{Q_{\max}r'+\pi}\right].$$

Our numerical implementation of this expression for $\tilde{g}_{md}(r)$ passed the "empty lattice test" of giving $\tilde{g}_{md}(r)=0$ when $g_{md}(r)=0$ with an accuracy of about one part in 10^2.

[1] B. Lin, J. W. Halley, and P. T. Boinske, J. Chem. Phys. **105**, 1668 (1996).
[2] F. M. Gray, *Solid Polymer Electrolytes* (VCH, New York, 1991).
[3] D. Rigby and R.-J. Roe, J. Chem. Phys. **87**, 7285 (1987).
[4] J. I. Mckechnie, D. Brown, and J. H. R. Clarke, Macromolecules **25**, 1562 (1992).
[5] D. Brown, J. H. R. Clarke, M. Okuda, and T. Yamazaki, J. Chem. Phys. **100**, 6011 (1994).
[6] S. Neyertz and D. Brown, J. Chem. Phys. **102**, 9725 (1995).
[7] J. A. Johnson, M.-L. Saboungi, D. L. Price, S. Ansell, T. P. Russell, J. W. Halley, and B. Nielsen, J. Chem. Phys. **109**, 7005 (1998).
[8] J. W. Halley and B. Nielsen, in *Materials for Electrochemical Energy Storage*, edited by D. S. Ginley, D. H. Doughty, T. Takamura, Z. Zhang, and B. Scrosati (Materials Research Society Proc. 1998), Vol. 496.
[9] R. Zbinden, *Infrared Spectroscopy of High Polymers* (Academic, New York, 1964), p. 148.
[10] R. L. Liboff, in *Elementary Quantum Mechanics* (Holden-Day Inc., San Francisco, 1980), p. 183.
[11] M. Zelen and N. Severo, in *Handbook of Mathematical Functions*, edited by M. Abramowitz and I. Stegun (Dover, New York, 1972), p. 952.
[12] A. Rahman and M. Parrinello, J. Appl. Phys. **52**, 7182 (1981).
[13] B. Brown and S. Neyertz, Mol. Phys. **84**, 577 (1995).
[14] W. J. Hehre, L. Radom, P. V. R. Schleyer, and J. A. Pople, *Ab Initio Molecular Theory* (Wiley, New York, 1986).
[15] W. Jorgenson and J. Tirado-Rives, J. Am. Chem. Soc. **110**, 3469 (1988).
[16] S. J. Weiner, P. A. Kollman, D. A. Case, U. C. Singh, C. Ghio, G. Alagona, S. Profeta, and P. Weiner, J. Am. Chem. Soc. **106**, 765 (1984).